PNAS Nexus, 2024, 3, pgae496
https://doi.org/10.1093/pnasnexus/pgae496
Advance access publication 12 November 2024
Research Report

Choroid plexus extracellular vesicle transport of blood-borne insulin-like growth factor 1 to the hippocampus of the immature brain

Niklas Ortenlöf[a], Suvi Vallius[a], Helena Karlsson[a,b], Claes Ekström[a,b], Amanda Kristiansson[a,b], Bo Holmqvist[c], Stanislava Pankratova[d,e], Norman Barton[f], David Ley[a,1] and Magnus Gram[a,b,g,*,1]

[a]Department of Clinical Sciences Lund, Pediatrics, Lund University, 22184 Lund, Sweden
[b]Department of Neonatology, Skåne University Hospital, 22184 Lund, Sweden
[c]Imagene-iT AB, 22381 Lund, Sweden
[d]Department of Veterinary and Animal Sciences, University of Copenhagen, 1870 Copenhagen, Denmark
[e]Department of Neuroscience, University of Copenhagen, 2200 Copenhagen, Denmark
[f]Scientific Advisory Board, Oak Hill Bio Ltd, Altrincham WA14 2DT, United Kingdom
[g]Department of Biomedical Science, Faculty of Health and Society, Biofilms—Research Center for Biointerfaces, Malmö University, 21432 Malmö, Sweden
*To whom correspondence should be addressed: Email: magnus.gram@med.lu.se
[1]D.L. and M.G. contributed equally to this work.
Edited By Andrey Abramov

Abstract

Reduced serum level of insulin-like growth factor 1 (IGF-1), a major regulator of perinatal development, in extremely preterm infants has been shown to be associated with neurodevelopmental impairment. To clarify the mechanism of IGF-1 transport at the blood–cerebrospinal fluid (CSF) barrier of the immature brain, we combined studies of in vivo preterm piglet and rabbit models with an in vitro transwell cell culture model of neonatal primary murine choroid plexus epithelial (ChPE) cells. We identified IGF-1-positive intracellular vesicles in ChPE cells and provided data indicating a directional transport of IGF-1 from the basolateral to the apical media in extracellular vesicles (EVs). Exposure of the ChPE cells to human IGF-1 on the basolateral side increased the secretion of IGF-1-positive EVs in the apical media. Mass spectrometry analysis displayed similarities in protein content between EVs derived from preterm piglet CSF-derived and ChPE cell–derived EVs. Furthermore, exposure of ChPE cells to human IGF-1 caused an enrichment of human IGF-1 and transmembrane p24 trafficking protein 2, proteins important for perinatal development, in apical media–derived EVs. Moreover, intraventricular injections of ChPE cell–derived EVs in preterm rabbit pups resulted in an uptake of EVs in the brain, displaying penetration through the ependymal lining and deep into the hippocampus. Finally, exposure of rat hippocampus neurons to ChPE cell–derived EVs resulted in internalization of the EVs in hippocampal soma and neurites. In summary, we describe a transport pathway for blood-borne IGF-1 in EVs through the blood–CSF barrier to the hippocampus in the immature brain.

Keywords: choroid plexus, extracellular vesicle, insulin-like growth factor 1, hippocampus, immature brain

Significance Statement

Neurodevelopmental impairment in extremely preterm infants is associated with reduced serum levels of insulin-like growth factor 1 (IGF-1), a major regulator of perinatal development. Elucidating the transport mechanism of circulatory IGF-1 to the immature brain is critical for our understanding of the body–brain interactions during development. Here, we show that blood-borne IGF-1 stimulates the secretion of IGF-1-positive extracellular vesicles (EVs) from the choroid plexus. We furthermore show that choroid plexus–derived EVs, containing IGF-1, are delivered to deep structures of the hippocampus in the immature brain. Our study suggests the presence of a transport pathway for EV-enclosed IGF-1, from the vascular compartment through the blood–cerebrospinal fluid barrier, and into the hippocampus of the developing brain.

Competing Interest: N.B. was employed by Takeda Pharmaceutical Company Ltd. and is a shareholder of Takeda Pharmaceutical Company Ltd. D.L. hold stock/stock options in Premalux AB and has received consulting fees from Shire PLC. All other authors declare no competing interests.
Received: November 24, 2023. **Accepted:** October 1, 2024
© The Author(s) 2024. Published by Oxford University Press on behalf of National Academy of Sciences. This is an Open Access article distributed under the terms of the Creative Commons Attribution-NonCommercial-NoDerivs licence (https://creativecommons.org/licenses/by-nc-nd/4.0/), which permits non-commercial reproduction and distribution of the work, in any medium, provided the original work is not altered or transformed in any way, and that the work is properly cited. For commercial re-use, please contact reprints@oup.com for reprints and translation rights for reprints. All other permissions can be obtained through our RightsLink service via the Permissions link on the article page on our site—for further information please contact journals.permissions@oup.com.

Introduction

Insulin-like growth factor 1 (IGF-1) has a crucial role in perinatal brain growth and development (1). However, extremely preterm (EPT) infants, i.e. born below gestational week 28, have been shown to exhibit low concentrations of circulating IGF-1 (2). Low levels of serum IGF-1 during development correlate with poor weight gain, lower brain volumes (3), and impaired cognitive development (4). IGF-1 is a mitogenic peptide, previously described to have a range of neuroprotective roles in cell proliferation and differentiation, as well as brain vessel stabilization (1, 5). Systemically administered IGF-1 has been shown to stimulate neurogenesis in the hippocampus in the preterm piglet (6). Furthermore, in a clinical trial, it was observed that restoring physiological serum IGF-1 levels in EPT infants, to levels corresponding to those of the healthy fetus remaining in utero, resulted in a trend toward decreased occurrence of severe intraventricular hemorrhage (7).

Although clinical data support that supplementary treatment with IGF-1 that restores physiological levels would have the potential to improve neurodevelopment, the molecular mechanisms underlying the protective effects are not fully understood. In particular, the route and mechanism(s) of transfer of IGF-1 from the circulation to the immature brain are not yet characterized. One potential site of transfer from blood to the parenchyma is via the choroid plexus (ChP) (8–10). The ChP is located at the interface between the vascular compartment and cerebrospinal fluid (CSF) and constitutes the blood–CSF barrier with tight junction proteins between the ChP monolayer epithelial cells (ChPE). The ChPE cells govern the production and secretion of CSF that provides adequate shock absorption, support, and nutrients to the central nervous system (CNS) (11). The transport of IGF-1 across the CSF barrier is described to involve the IGF-1 receptor (IGF-1R), which is expressed abundantly in the ChPE (5, 8–10, 12). However, the understanding of how IGF-1 is further carried through the ChPE cells, via the CSF, and into the brain parenchyma is currently not well understood.

The ChP produces and releases extracellular vesicles (EVs) into the CSF, followed by an uptake into the parenchyma (13, 14). EVs are nano-sized, cell-derived phospholipid membrane–enclosed vesicles that are mainly comprised of nucleotides, proteins, and lipids from the cell of origin (15). EVs have been described to constitute important cell-to-cell messengers with the ability of regulating diverse cellular functions of recipient cells (16).

In the present study, we hypothesized that exposure of ChPE cells to circulating IGF-1 would lead to an uptake of IGF-1 and an encapsulation into EVs, induce an increased EV secretion, and potentially modify the cargo of the EVs. By combining in vivo preterm piglet and rabbit models with an in vitro transwell neonatal ChPE cell culture model, we describe transport of human IGF-1 in EVs through the blood–CSF barrier, via the CSF, and into the hippocampus of the immature brain.

Results

IGF-1 is localized in intracellular vesicles in a neonatal primary murine ChPE transwell cell culture model

To characterize how circulating human IGF-1 (hIGF-1) affects neonatal ChPE cell secretion of EVs and its content, we established a transwell in vitro cell culture system using postnatal day 3–8 primary murine ChPE cells. In this system, exposure from the circulation can be mimicked from the basal side, whereas the CSF side is represented by the apical side; see a schematic illustration of the in vitro study outline in Fig. 1A. The cells were cultured as describe previously (17), and the model was characterized by verifying positive expression of the ChPE marker transthyretin (TTR, green) and the tight junction protein zonula occludens-1 (ZO-1, red) (SI Appendix, Fig. S1A and B, respectively) (18). Additionally, absence of fibroblast contamination was confirmed by labeling with S100A4 and heat-shock protein (Hsp) 47 (SI Appendix, Fig. S1C and D) (19, 20). Moreover, the formation of a blood–CSF barrier was confirmed by transepithelial electrical resistance (TEER) measurements and conducting a transcytosis assay (SI Appendix, Fig. S1E and F) (21). Following exposure to 40 ng/mL hIGF-1 on the basal side for 24 h, a presence of IGF-1 was observed within the cultured ChPE cells using confocal light microscopy (Fig. 1B middle left). Furthermore, labeling against IGF-1R also displayed positive signals within the ChPE cells (SI Appendix, Fig. S2). Interestingly, co-labeling with the late endosomal marker CD63, characteristic for multivesicular bodies (22), displayed co-localization with IGF-1, IGF-1R, and TTR, indicating intracellular vesicle location of IGF-1, its receptor, and TTR (Fig. 1B far right and SI Appendix, Fig. S2). Moreover, transmission electron microscopy (TEM) immunogold labeling of the exosomal marker flotillin-2 displayed presence of intracellular membrane–enclosed vesicles (Fig. 1C, white arrows), indicating production of EVs (20). In addition, immunogold labeling against IGF-1 revealed an accumulation in intracellular membrane–enclosed vesicles and an indication of IGF-1-positive vesicles release into the extracellular space (Fig. 1D and E, white arrows and SI Appendix, Fig. S3A–C, white arrows). An accumulation of IGF-1 was also visible in the ChPE mitochondria (SI Appendix, Fig. S3B). Of note, it was not feasible to determine whether the IGF-1 retained within the vesicle was hIGF-1 or murine IGF-1 as the antibody used detects both epitopes.

ChPE cells secrete IGF-1-positive EVs upon hIGF-1 stimulation

Next, we aimed to evaluate whether hIGF-1 is transported from the ChPE cells in intracellular vesicles to the extracellular space. The neonatal primary murine ChPE cells were exposed to hIGF-1 (40, 100, and 250 ng/mL) at the basal side for 24 h, and the supernatant at the apical side was collected for subsequent EV preparation and analysis. Successful preparation of EVs was verified by TEM analysis and confirmed presence of exosomes, by showing positive labeling for the exosomal marker flotillin-2, in the ChPE cell–secreted supernatant (Fig. 2A and SI Appendix, Fig. S3E). TEM analysis of IGF-1, using immunogold labeling, displayed presence on/in the purified vesicles, both larger and smaller vesicles (Fig. 2B and SI Appendix, Fig. S3F). Of note, separation of hIGF-1 and murine IGF-1 was not feasible as the antibody used detects both epitopes. Subsequently, we analyzed the amount of EVs released into the apical supernatant, measured by nanoparticle tracking analysis (NTA), following exposure of ChPE cells to 40, 100, and 250 ng/mL of hIGF-1. Exposure to 40 ng/mL hIGF-1, but not 100 and 250 ng/mL, displayed a significant increase of ChPE cell–released EVs as compared to control (Fig. 2C and D). Based on these results, 40 ng/mL hIGF-1 was used in subsequent experiments. To further support that IGF-1 is retained in ChPE cell–derived EVs, we inhibited EV secretion from the ChPE cells by adding GW4869, a well-established inhibitor of neutral sphingomyelinase involved in EV production (14, 23). Inhibiting EV production indicated a reduction of IGF-1 concentration in the ChPE cell–derived EVs (SI Appendix, Table S1).

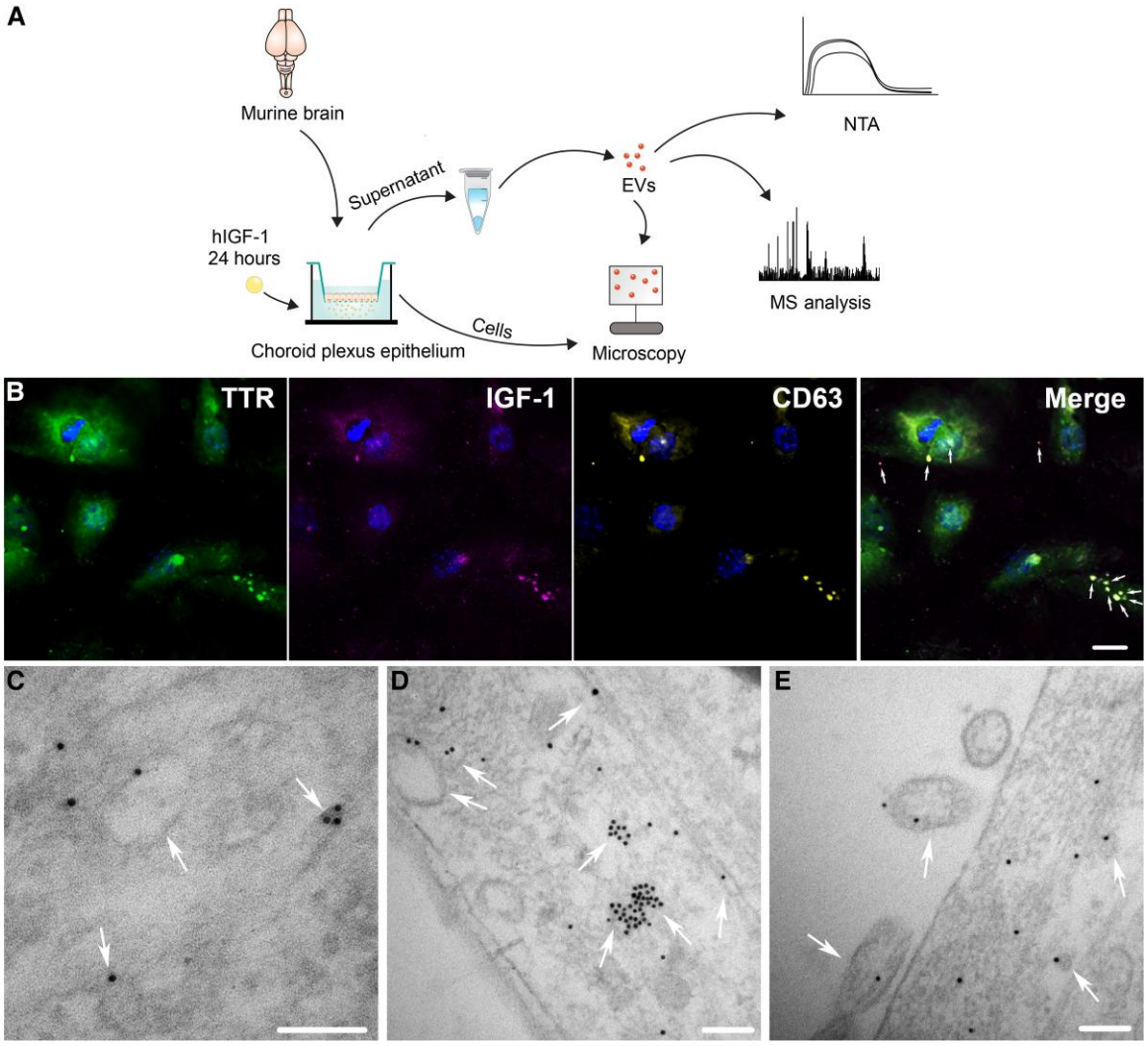

Fig. 1. Localization of IGF-1 in neonatal primary murine ChPE cells. A) Schematic illustration of the in vitro study outline. B) Representative confocal microscopy images illustrating labeling of TTR (green, B, far left and far right), IGF-1 (magenta, B, middle left and far right), and CD63 (yellow, B, middle right and far right) in neonatal primary murine ChPE cells cultured in the transwell system. Co-localization of IGF-1 with the late endosomal marker CD63 is displayed by white arrows in the merged image (B, far right). The scale bar represents 20 μm and is representative for all images in B. C–E) Representative TEM images illustrating immunogold labeling of flotillin-2 (C) and IGF-1 (D–E) in neonatal primary murine ChPE cells cultured in the transwell system. White arrows display IGF-1 and flotillin-2 immunogold labeling in membrane-enclosed vesicles. The scale bars in C–E represent 100 nm. Confocal microscopy and TEM images are collected from three independent experiments.

Proteomic analysis reveals presence of hIGF-1 in ChPE cell–derived EVs upon hIGF-1 stimulation

Next, we asked whether the proteome, obtained by mass spectrometry (MS) analysis, of EVs, purified from ChPE cell supernatant, would alter following hIGF-1 exposure. Overall, hIGF-1 induced marginal effects when the criterion for significance was set to an adjusted *P*-value (Benjamini–Hochberg-corrected *P*-value ≤ 0.05) (Fig. 3A). Interestingly, hIGF-1 and transmembrane p24 trafficking protein 2 (Tmed2), important for in utero embryonic development (24), were significantly enriched (Fig. 3A, yellow dots, and B). Next, we submitted proteins with less strict criteria for significance (log fold-change ≥ 1 and ≤ −1, and *P*-value ≤ 0.05) (Fig. 3A, red and light blue dots) to Metascape. The outputs displayed enrichment of pathways involved in cellular response to amyloid-beta, regulation of translation, regulation of post-synaptic organization, and regulation of cell morphogenesis following hIGF-1 stimulation (Fig. 3C). Suppressed pathways in ChPE cell–derived EVs upon hIGF-1 stimulation were formation of the cornified envelope and intermediate filament organization (Fig. 3C).

EV proteomes are similar between ChPE supernatant and preterm piglet CSF

To expand our understanding of the impact of hIGF-1 on the ChP-secreted EVs, we investigated whether the hIGF-1-exposed ChPE cell–derived EV proteomes share similarities with that of EVs derived from preterm piglet CSF. Preterm piglets, delivered by cesarean section (c.s.) at a gestational age of 106 days (full term = 117 days), were exposed to recombinant hIGF-1 (in complex with IGF-1-binding protein 3, IGFBP-3, and henceforth referred to as hIGF-1, 2.25 mg/kg/day via subcutaneous injections), or the corresponding vehicle solution (control group) for 9 days, and CSF samples were collected at termination (25). Analysis of the proteome, using MS analysis with significance criteria set to adjusted *P*-value (Benjamini–Hochberg-corrected *P*-value ≤ 0.05), displayed a

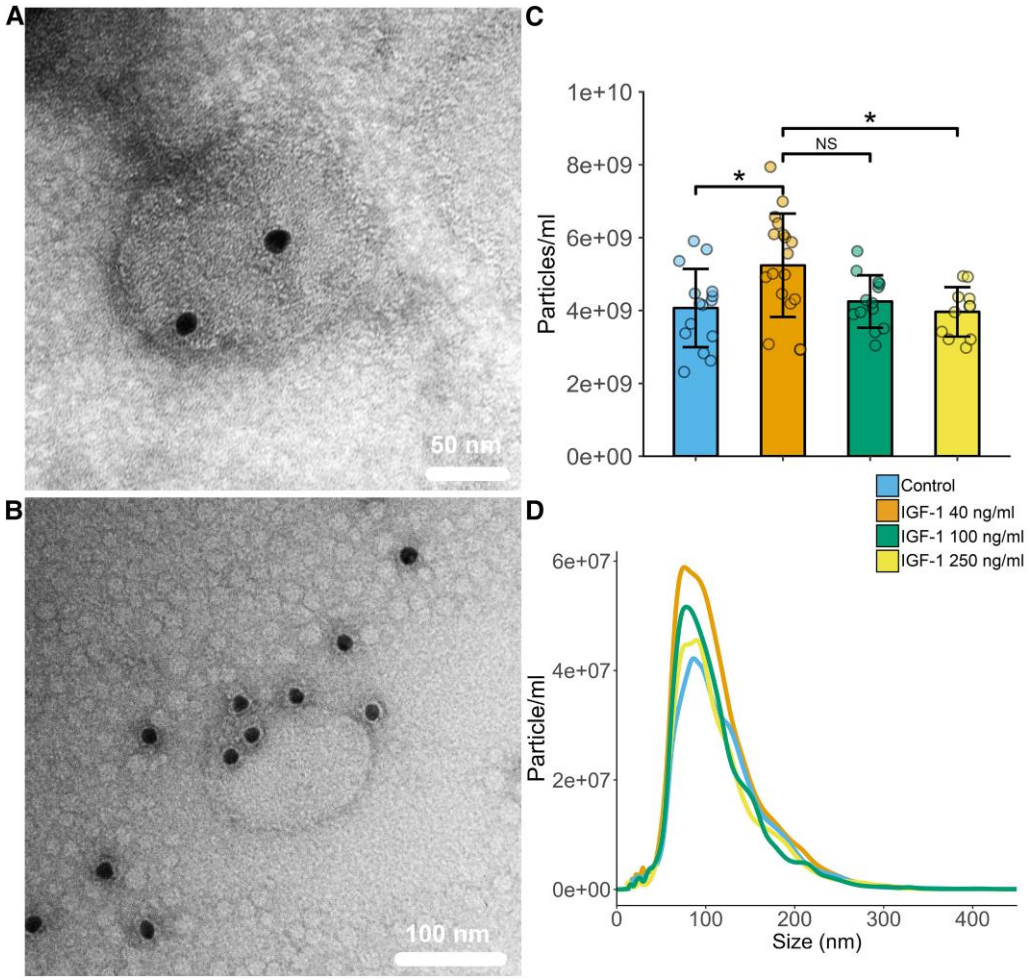

Fig. 2. IGF-1-positive vesicles are released from ChPE cells following hIGF-1 stimulation. Representative TEM image of purified neonatal primary murine ChPE cell–derived EVs immunogold labeled with flotillin-2 (A) and IGF-1 (B). NTA quantification (C), and size distribution (D) of EVs secreted into the apical supernatant of the ChPE cells following exposure to hIGF-1 (40, 100, and 250 ng/mL) for 24 h. Data are from four independent experiments with $N = 4$–6 at each respective experiment. Data are presented as mean ± SD. Differences between 40, 100, and 250 ng/mL hIGF-1 vs. control were analyzed using one-way ANOVA with a post hoc Tukey test for multiple comparisons of means, $^*P \leq 0.01$.

similar pattern as the ChPE cell–derived EVs with only minor changes in the proteome following hIGF-1 exposure (Fig. 4A). In line with ChPE cell–derived EVs, submitting proteins with less strict significance criteria (log fold-change ≥ 1 and ≤ −1, and P-value ≤ 0.05) to Metascape identified additional pathways, including a suppression of intermediate filament organization upon exposure to hIGF-1 (Fig. 4B), further supporting the similarities between the two proteome datasets. Of note, no enriched pathways were found in EVs derived from preterm piglets CSF upon IGF-1 treatment.

Inspecting the total proteome of all conditions comparing proteins identified in ChPE cell–derived EVs (1,396 unique proteins) and preterm piglets CSF-derived EVs (1,759 unique proteins), we observed a 50–60% overlap between the proteomes (Fig. 4C). To identify the pathways enriched in the proteome of the EV samples, we performed a pathway analysis using Metascape (26). Of the top 20 enriched pathways, five of the Reactome gene sets (27) and two of the GO biological process (28) were similarly enriched comparing the two datasets (Fig. 4D). One of the top enriched Reactome pathways for both datasets was vesicle-mediated transport (Figs. 3B and 4D), and 17–18 of the top 19 most common EV markers, published on the Vesiclepedia website (http://microvesicles.org/index.html) (29, 30), were identified in both datasets (SI Appendix, Table S2), indicating successful EV preparation from the ChPE supernatant and preterm piglet CSF. The raw dataset for MS data is accessible in S2–S3 Appendix.

ChPE cell–derived EVs penetrate into the hippocampus of the preterm rabbit brain

Previous studies have shown an uptake of EVs derived from ChPE cells into the brain parenchyma (13, 14). Based on this and our findings here, we further aimed to investigate whether there is a delivery of hIGF-1-stimulated ChPE cell–derived EVs into subcortical structures in the immature brain. Thus, utilizing our preterm rabbit pup model, we investigated the distribution of purified and labeled ChPE cell–derived EVs in the immature brain following intracerebroventricular (i.c.v.) injection. EVs, prepared from hIGF-1 or vehicle (control) exposed neonatal primary murine ChPE cells in vitro, were stained with general membrane label PKH26 and subsequently i.c.v. injected (ultrasound-guided) into the lateral ventricles of nonsedated preterm rabbit pups (see SI Appendix, Fig. S4 for visualization of the injection using the high-frequency ultrasound). Pups were terminated 4.5 h after the i.c.v. injection,

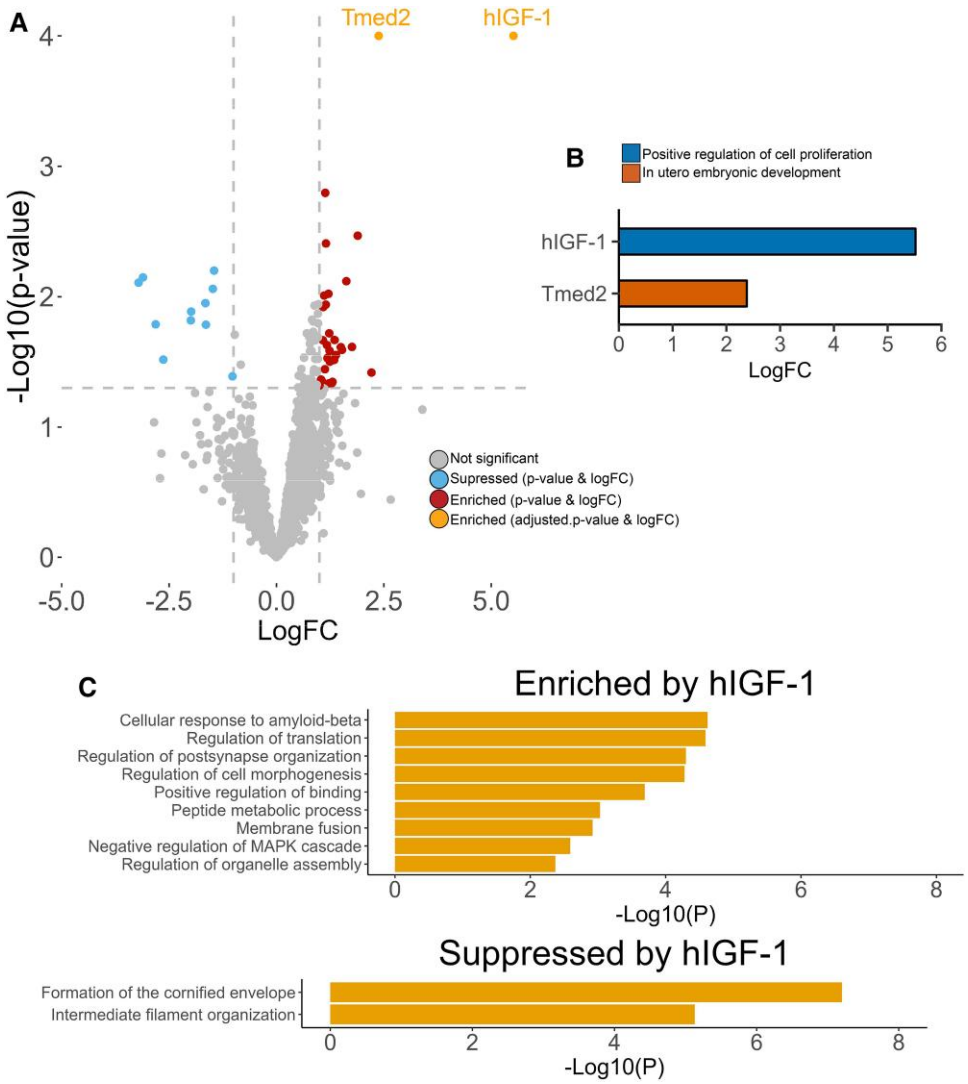

Fig. 3. Proteome analysis of EVs derived from ChPE cells upon hIGF-1 stimulation. A) Volcano plot of the proteome in EVs derived from ChPE cells exposed to 40 ng/mL IGF-1 as compared to control cells. B) Significant changes in abundance of proteins identified in EVs derived from ChPE cells, with the significance criteria fold-change ≥1.5 and ≤−1.5, and adjusted *P*-value, Benjamini–Hochberg-corrected *P*-value ≤ 0.05, following hIGF-1 (40 ng/mL) stimulation. GO biological processes terms based on David analysis for individual proteins are displayed. C) Metascape analysis of enriched (upper) and suppressed (lower) proteins identified in EVs derived from ChPE cells following exposure to 40 ng/mL hIGF-1. The significance criteria used were, log fold-change ≥1 and ≤−1, and *P*-value ≤ 0.05.

and brains were collected and cryosectioned, and the PKH26 fluorescence signal was analyzed with confocal microscopy (see Fig. 5A for a schematic illustration of the experimental outline). The analysis showed the presence of vesicle- or organelle-like structures, corresponding to EVs beyond the ependymal lining of the hippocampus (Fig. 5B and C) and into deeper layers of the hippocampus, reaching the pyramidal and the molecular levels in the cornu ammonis (CA)2–CA3 region (Fig. 5D). No difference was found in EV uptake comparing EVs derived from hIGF-1-stimulated or control ChPE cells (Fig. 5C and D). Injection of only PKH26 dye resulted in negligible signal in investigated regions (SI Appendix, Fig S5).

ChPE cell–derived EVs are internalized by hippocampal neurons in vitro

To further characterize the EV-mediated interaction between the ChP and the hippocampus, we performed an EV uptake experiment in vitro. Primary rat hippocampal neurons were incubated with purified neonatal primary murine ChPE cell–derived EVs labeled with the membrane label PKH67. Following exposure for 2 h, the neurons were fixed, fluorescence-labeled with antibodies against GAP-43, and analyzed by confocal microscopy; see Fig. 5A for a schematic illustration of the experimental outline. As displayed in Fig. 5E, EVs were observed to be readily taken up by the cells, localized in the soma and in the neurites. Furthermore, comparing uptake in neurons exposed to hIGF-1-stimulated ChPE cell–derived EVs vs. EVs from unstimulated control ChPE cells showed a trend ($P = 0.07$) of increased uptake following hIGF-1 stimulation (Fig. 5F). Hippocampal neurons exposed to only PKH67 showed dye uptake, but the intracellular distribution was vastly different from neurons exposed to PKH67-stained EVs (SI Appendix, Fig. S6A). No PKH67 signal was detected in neurons exposed to phosphate-buffered saline (PBS, SI Appendix, Fig. S6B).

Discussion

IGF-1 has a paramount role in numerous processes, including proliferation, gene expression, inhibition of apoptosis, oxidative stress, and protein translation (1, 5, 31). Additionally, IGF-1

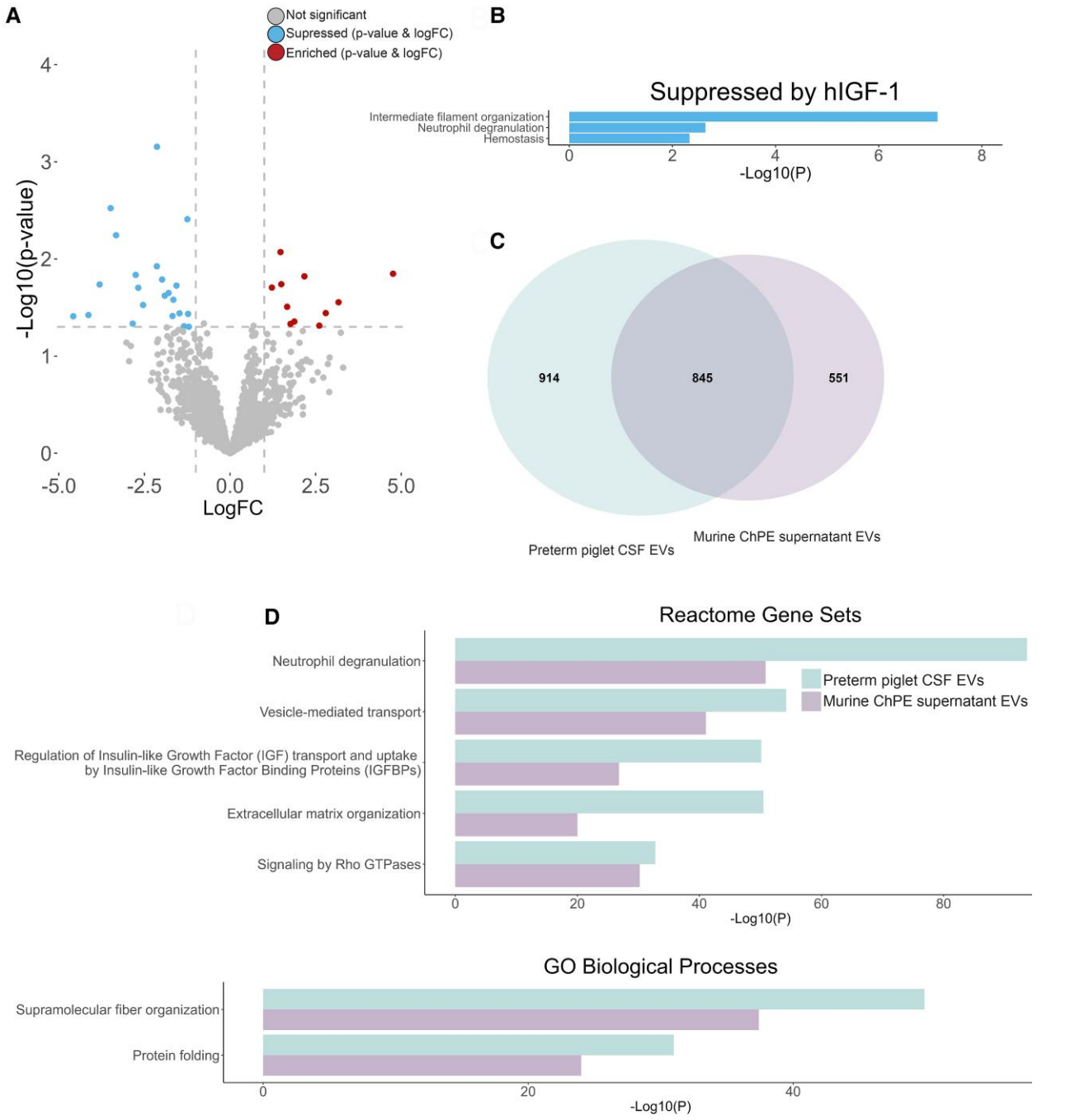

Fig. 4. Proteome analysis of ChPE cell–derived EVs and preterm piglet CSF-derived EVs. A) Volcano plot of the proteome in preterm piglet CSF-derived EVs exposed for 9 days to hIGF-1 (2.25 mg/kg/day) compared with vehicle-treated (control group) piglets. B) Metascape analysis of suppressed proteins identified in EVs derived from preterm piglet CSF upon hIGF-1 treatment with the significance criteria log fold-change ≥1 and ≤−1 and *P*-value ≤ 0.05. C) Venn diagram displaying overlap of proteins derived from ChPE cell supernatant EVs (purple, $N = 12$) or preterm piglet CSF EVs (green, $N = 16$). D) Reactome gene sets (upper) and GO biological processes (lower) using Metascape of proteome in EVs derived from ChPE cell supernatant or preterm piglet CSF. Results are retrieved from the top 20 hits using Metascape.

mediates neuronal growth and angiogenesis and is crucial for fetal brain development (32). Low serum IGF-1 levels following premature birth have been associated with increased rates of impaired neurodevelopmental outcomes (3). Therefore, elucidating the transport mechanism of circulatory IGF-1 to the brain is pivotal for further understanding the interaction between body and brain during development. The ChP is regarded as the gateway to the brain (33) and the primary route for peripheral IGF-1 to enter the CNS (5, 8). Here, we describe the ChP as a route of passage for blood-borne IGF-1 into deep parts of the parenchyma of the developing brain, including the hippocampus. We show that the transport of IGF-1 could occur via ChPE cell–derived EVs. In addition, our experiments indicate that IGF-1 influences the secretion of ChPE cell–derived EVs, increasing the amount of both EVs secreted and the cargo carried.

The receptor for IGF-1 is abundantly expressed across the ChP, providing a possible ligand–receptor interaction of IGF-1 at the blood–CSF barrier that enables interaction from both the CSF

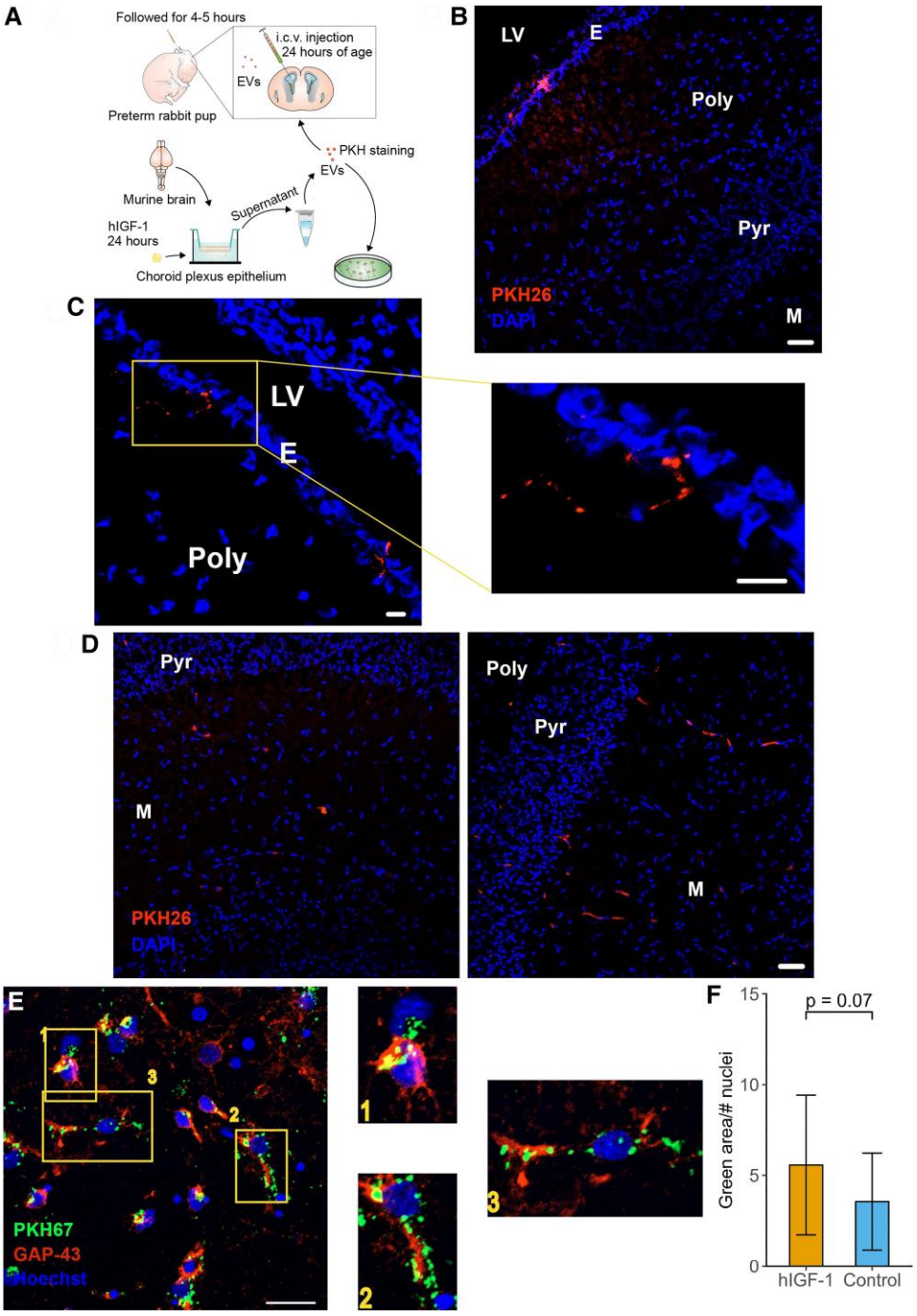

Fig. 5. In vivo and in vitro hippocampal uptake of ChPE cell–derived EVs. A) Schematic illustration of the experimental outline. B)–D) Representative confocal microscopy images illustrating presence of ChPE cell–derived EVs stained with the dye PKH26 (red) in the hippocampus of the preterm rabbit pup brain following i.c.v. injections. B) and C) Representative images illustrating EVs beyond the ependymal layer in the polymorph layer. D) Representative images illustrating EVs in deep structures of the CA2–CA3 regions of the hippocampus proper in the pyramidal layer and further in the molecular layer. Representative images were collected from $N = 8$. The scale bars in B–D represent 50 μm. E) Representative confocal microscopy image of GAP-43-labeled (red) rat hippocampal neurons incubated with ChPE cell–derived EVs stained with PKH27 (green). The scale bar in E represents 25 μm. F) Quantification of green signal per number of nuclei (DAPI stained, blue) in hippocampal neurons exposed to EVs derived from hIGF-1-stimulated ChPE cells was obtained from representative areas of all wells ($N = 12$ wells per condition). Data are presented as means ± SD. Differences between groups were analyzed using Student's t test. E) ependymal layer; Poly, polymorph layer; Pyr, pyramidal layer; M, molecular layer; LV, lateral ventricle; DAPI, 4′,6-diamidino-2-phenylindole.

and the blood side (10, 12). Pulford et al. (34) have, however, previously shown that the uptake of IGF-1 from circulation is non-IGF-1R or binding protein dependent. Furthermore, we have observed an abundance of the IGF-1R on the CSF-facing side of the ChP rather than the blood side (10, 12), suggesting a putative non-IGF-1R or binding protein transportation of IGF-1 from the periphery to the CSF. The transportation of IGF-1 could be within EVs, as the ChP has been shown to produce and release EVs, enabling delivery of molecules such as nutrients and miRNAs to the surrounding parenchyma (13, 14). Consequently, in this study, we hypothesized that the transport of IGF-1 from the circulation to the immature brain may involve uptake of IGF-1 via

endocytosis in the ChP and a subsequent EV secretion into the CSF. The transport of IGF-1 from the blood to the brain, via interaction with the ChP, has been studied in the adult context previously (9, 35). For instance, Carro et al. showed that the ChP is the main route of uptake from blood to the parenchyma in an adult mice exercise model (8, 36). However, to the best of our knowledge, this study is the first to investigate the effects of IGF-1 on EV formation and secretion from the ChP in the context of the immature brain. We observed an uptake and accumulation of IGF-1 in membrane-enclosed vesicles in the ChPE cells, a translocation of IGF-1 through the ChPE via intracellular vesicles to the apical supernatant, and a secretion of IGF-1-positive EVs into the apical culture medium, i.e. corresponding to the CSF. We further attempted to elucidate whether the ChP mediates this transfer and observed an indication of a reduction in ChPE cell–derived EVs following inhibition of EV release. Interestingly, we also observed that intracellular vesicles carrying IGF-1 displayed positive immunolabeling for the IGF-1R, indicating that packaging of IGF-1 may occur together with its receptor.

To investigate the relevance of the in vitro EV-IGF-1 transport findings, we characterized the proteome content of the ChPE cell–derived EVs and compared it to that of the proteome of preterm piglets CSF-derived EVs, following exposure to hIGF-1 in respective system. Interestingly, the analysis displayed large similarities between the two datasets, including that 60% of the proteomes were identical, and the pathway of vesicle-mediated transport was enriched in both datasets. Thompson et al. have shown that a major proportion of CSF proteins within EVs have a ChP origin in human adults (37), and here, we provide additional data to support this. Although globally, we observed only minor differences in the proteome of both datasets, comparing hIGF-1 stimulation vs. nonstimulated, one major finding was that hIGF-1 was enriched in EVs derived from hIGF-1-stimulated ChPE cells, thus proving further evidence of IGF-1 transport in EVs through the blood–CSF barrier.

Based on the observation that EVs are secreted into the apical supernatant, i.e. into a compartment corresponding to the CSF, we further hypothesized that the CSF-secreted EVs, with encapsulated IGF-1, are destined for transportation of IGF-1 to recipient cells beyond the ventricular ependyma. Previous studies, Grapp et al. and Balusu et al., have in fact shown in a murine adult brain that ChP-derived EVs penetrate the ependymal lining of the ventricles followed by an uptake in astrocytes and microglia (13, 14). Grapp et al. further showed how the secretion of EVs from the ChPE to the CNS provides nutrients from the blood to the CNS (13). In addition, Balusu et al. showed that certain systemic stimuli, such as inflammation, enhanced the EV formation and secretion from the ChPE (14).

However, to the best of our knowledge, a potential distribution of the ChPE cell–derived EVs to a specific subcortical structure of the immature brain has not been investigated. Importantly, previous studies investigating distribution of i.c.v. injected EVs have used sedated animals (13, 14, 38, 39). Sedation is, however, well known to significantly affect circulation and perfusion of the brain (40, 41). In this study, we therefore performed ultrasound-guided i.c.v. injections of ChPE cell–derived EVs in nonsedated preterm rabbit pups, a model highly suitable and widely used for studies of the immature brain (42–45). We detected EVs deep into the hippocampus, including the deeper layers of the pyramidal and molecular layer of the CA2–CA3 region. To further substantiate and characterize this finding, we investigated the ability of primary hippocampal neurons to take up purified ChPE cell–derived EVs in an in vitro setting. We observed that hippocampal neurons

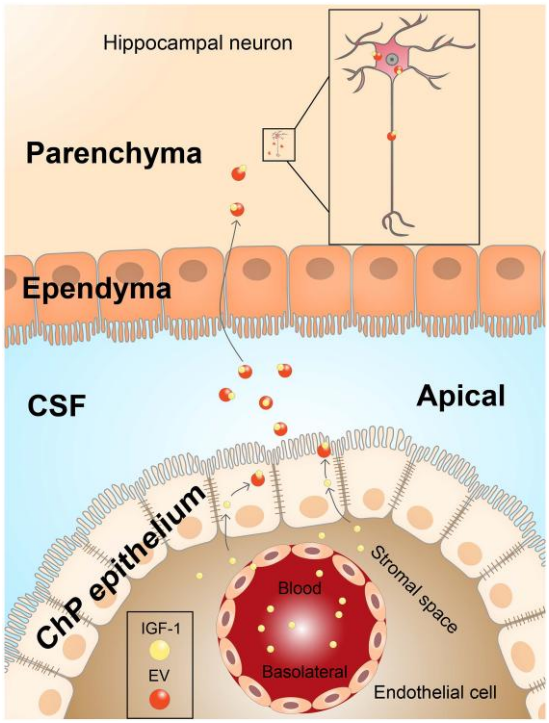

Fig. 6. Schematic illustration describing the suggested model of IGF-1 transport. The ChP constitutes the barrier between the periphery and the CSF of the brain. This highly secretory organ enhances EV-secretion following exposure to systemic IGF-1. The blood-borne IGF-1 is transported through the blood–CSF barrier, encapsulated in EVs secreted from the ChP, ultimately reaching the hippocampus in the immature brain.

displayed an extensive uptake of EVs purified from ChPE cells localized in the cell body soma and in the neurites. Altogether, this indicates a targeted delivery of the ChP-derived EVs to the hippocampus of the immature brain. The effect of this delivery has not been studied here. However, considering the change in proteome of the ChP-derived EVs following IGF-1 exposure, it could be speculated that these EVs may induce enhanced hippocampal neurodevelopment. This notion is further supported by the finding of Christiansen et al., who reported that preterm piglets exposed to systemic IGF-1 displayed an increased density of neurons in the hippocampus (6). The authors also reported changes in gene expression related to glial and neuronal maturation, including Opalin, AQP4, TTR, and EEF1A2, in the hippocampus of preterm piglets following systemic IGF-1 exposure. Thus, further studies are needed to establish the entire physiological potential IGF-1 has on the developing brain.

There are important aspects to the current study that should be considered, foremost, a major proportion of the data presented is derived from primary neonatal murine ChPE cells. Future studies should thus focus on translating the findings to human settings, for instance, by using primary cells or induced pluripotent stem cells. In the current study, we attempted to evaluate the presence of IGF-1 in EVs derived from CSF collected from preterm infants diagnosed with intraventricular hemorrhage. However, using ELISA-analysis, IGF-1 was not detected in any of the six patients, most likely due to insufficient sample availability. Future studies should therefore consider using more sensitive methods, such as MS, to confirm whether IGF-1 is present within EVs derived from human CSF. Our data suggesting hippocampal neuronal uptake of ChPE cell–derived EVs are primarily based on our in vitro uptake

studies. Future studies could strengthen this claim by labeling neural markers in the hippocampus and evaluating co-localization with the ChPE cell–derived EVs in vivo, following i.c.v. injections of stained ChPE cell–derived EVs.

In summary, this study suggests a mechanism for EV-encapsulated IGF-1 transport through the blood–CSF barrier and beyond the ependymal lining into the hippocampus of the developing brain (as depicted in Fig. 6). The impact of IGF-1 on the immature brain as well as the functions of EV-mediated communication from the ChP to the surrounding parenchyma requires more research as they may provide opportunities for supporting neurodevelopment following EPT birth.

Materials and methods

Animals

Preterm rabbit pups

The animal protocols were approved by the Swedish Animal Ethics Committee in Lund (Dnr: 5.8.18-06020/2019). We utilized a well-established preterm rabbit pup model in accordance with the previous description (10, 42, 46) using New Zealand White rabbits (Egle Kergiene, Lundsbrunn, Sweden). In brief, the study involved nine rabbit pups from seven litters (four females and five males) delivered by cesarean section after the does were anesthetized with intravenous Propofol-Lipuro (20 mg/mL, B. Braun Melsungen AG, Germany) on gestational day 29 (term is 31–32 days). Following delivery, the pups were cared for by laboratory staff, dried, and placed in an infant incubator set to 30 °C and 60% humidity. At 1–2 h of age, the pups were weighed, marked, and hand-fed with bovine colostrum (100 mL/kg/day, Biodane Pharma, Gesten, Denmark) via a four French feeding tube (Vygon, Ecouven, France). At 12 h of age, the pups were fed a 1:1 mixture of bovine colostrum and Fox Valley 30/50 milk replacement formula (Melk voor Dieren, Rotterdam, The Netherlands). From 24 h onward, they were fed exclusively Fox Valley 30/50, with the amount increased by 10 mL/kg/day every 24 h. Feedings at 12, 36, and 60 h were halved from the previous dose (e.g. 50 mL/kg at 12 h after receiving 100 mL/kg at birth). The pups were gently cleaned once or twice daily as needed to maintain hygiene.

Preterm piglets

All animal procedures were performed in accordance with the Danish National Committee on Animal Experimentation (license no. 2014-15-0201-00418). Preterm piglets were delivered by c.s. at 106 days of gestation (full term = 117 days), housed in individual incubators, and reared to 9 days (P9) as previously described (6). Pigs were treated with either recombinant human (rh)IGF-1/rhIGFBP-3 complex (2.25 mg/kg/d; mecasermin rinfabate, Takeda, Boston, MA, USA) or the corresponding vehicle (control group) via subcutaneous injections three times per day until P9. Detailed feeding regimen and physiological, behavioral, and clinical responses following the rhIGF-1/rhIGFBP-3 treatment are reported in separate articles (6, 25). Pigs were anesthetized and then sacrificed with intracardiac injection of sodium pentobarbital followed by immediate collection of CSF by suboccipital puncture. The CSF was centrifuged at 2,500×*g* at 4 °C for 10 min, visually inspected for stick bleedings (to exclude blood contamination), and stored at −80 °C.

Primary ChPE cell cultures

The animal protocols were approved by the Swedish Animal Ethics Committee in Lund, Sweden (Dnr. 5.8.18-12930/2019). Primary murine ChPE cell culture studies were performed as previously described (10, 17). In brief, brains from 3- to 8-day-old mice pups (C57Bl/6Ncrl, Scanbur, Karlslunde, Denmark) were isolated. ChP from the lateral and fourth ventricles was isolated under a dissection microscope (Nikon SMZ800N Stereomicroscope, Tokyo, Minato, Japan). Cells were dissociated by an enzymatic reaction with 2 mg/mL pronase (isolated from *Streptomyces griseus*, Merck, Burlington, MA, USA). The reaction was terminated by the addition of excess complete DMEM-F12 cell culture medium (Gibco, Waltham, MA, USA) containing 10% fetal bovine serum (FBS, Gibco) and 1% Antibiotic-Antimycotic (Gibco). The cells were then centrifuged 1,000×*g* for 2 min, resuspended in DMEM-F12 culture medium, and plated (10^5 cells/well) on a 12-well transwell system (CLS3460-48EA, Sigma, Merck, Solna, Sweden). Cells were incubated at 37 °C in 5% CO_2 for 8–9 days. To eliminate fibroblast contamination, the culture medium was replaced after 48 h with complete DMEM-F12 medium supplemented with cytosine arabinoside (Ara-C, Merck). Subsequently, the complete DMEM-F12 medium was changed every 48 h. Functional characteristics of the ChPE cells were ascertained by positive labeling for TTR and ZO-1, absent labeling for fibroblast markers (S100A4 and Hsp47), and an increasing TEER during culture.

Transepithelial electric resistance

TEER analysis was performed to ensure that ChPE cells retained/established blood–CSF barrier function and was conducted using the EVOM2 (World Precision Instruments, Sarasota, FL, USA). The probes were sterilized by incubating for 15 s to 1 min in 70% ethanol and washing with PBS (pH 7.4). Identical sterilization steps were performed between every TEER measurement. TEER measurement of wells containing only complete DMEM-F12 cell culture medium was used as blank and subtracted from all measurements. The filter membrane diameter was multiplied to all blank subtracted measurement, and the electric resistance was expressed as $\Omega.cm^2$.

Diffusion assay

To further confirm an established blood–CSF barrier at the ChPE cells, diffusion assay analysis was conducted. ChPE cell cultures were prepared as described in section "Primary ChPE cell cultures." Transwells, coated with ChPE cells, were transferred to a new transwell multiwell plate, and 800 µL phenol red-free MEM (Gibco) was added to the basolateral compartment. The cell culture medium (MEM) of the apical compartment was replaced with 250 µL of 1 mg/mL 20 kDa FITC-Dextran solution (Merck). The ChPE cells were incubated, protected from light, at room temperature for 20 min. Subsequently, the basolateral media were collected and 100 µL aliquots transferred to a 96-well microtiter plate in triplicates, and the plate was read at 490 (excitation) and 520 nm (emission) using a VICTOR3 plate reader (Perkin Elmer, Waltham, MA, USA).

IGF-1 exposure of ChPE cell cultures

After 8–10 days of culturing, the ChPE cells reached an electrical resistance of 80–110 $\Omega.cm^2$ and, as described previously, were suitable for experimental procedures (14). The cells were cultured in complete DMEM-F12 containing 10% exosome-depleted FBS (Gibco), for ~24 h, and subsequently, cell culture medium was changed 4 h before IGF-1 exposure to fresh DMEM-F12 media containing 2% exosome-depleted FBS. Human IGF-1, 40, 100, or 250 ng/mL (R&D systems, 291-G1, Minneapolis, MN, USA) was

added to the basolateral side of the culture dish (corresponding to the circulatory/blood compartment), and the ChPE cell culture was continued for 24 h. For the inhibitor test, neutral sphingomyelinases inhibitor GW486 (Sigma) 10 μM in DMSO was added apical side of the culture dish. Subsequently, the apical supernatant (corresponding to the CSF compartment) and the basolateral supernatant were collected and stored at −80 °C until subsequent EV preparation and analysis. The analyses included the proteome, surface marker, and brain uptake of ChPE cell–derived EVs both in vivo and in vitro; see sections "EV preparation," "EV number and size measurements," "Electron microscopy," "Liquid chromatography–MS," "In vivo intraventricular brain injections," "IGF-1 concentrations," and "In vitro EV uptake experiment with hippocampal neurons" for further details.

EV preparation

To prepare EVs from ChPE cell culture supernatant and piglet CSF, the miRCURY exosome kit (Qiagen, Hilden, North Rhine-Westphalia, Germany) was used according to the manufacturer's instructions. In brief, samples were centrifuged at 3,000×*g* for 8 min to remove debris. Precipitation media (0.4 precipitation media volume × sample volume) were added to the sample and incubated overnight at 4 °C. The precipitation solution was then centrifuged at 10,000×*g* at 20 °C, and the sample was carefully aspirated and stored at −80 °C. The remaining EV pellet was either (i) directly stored at −80 °C (for subsequent MS and IGF-1 concentration analysis) or (ii) resuspended in 40–100 μL of suspension media and stored at −80 °C (used for surface marker analysis using TEM), or further prepared for NTA.

EV number and size measurements

To determine EV size and concentration, NTA was used. In brief, EVs were prepared as described above and subsequently diluted 1:10 in PBS and injected into NanoSight (LM14C, Malvern Panalytical, Malvern, United Kingdom). All samples were recorded for 90 s in triplicate with a camera level of 15 and a detection threshold of 5. Absolute numbers were calculated with the acquisition software (NTA version 3.3, Malvern Panalytical).

IGF-1 concentrations

40 μL lysis buffer (1 mM EDTA, 1 mM EGTA, 5 mM Na-pyro-phosphate, 0.27 M sucrose, 50 mM NaF, 50 mM Tris–base, 1 mM Na-orthovanadate, and 1% w/v NP40) containing freshly added protease inhibitor cocktail and 1 mM dithiothreitol (DTT) was added to the samples as described in "EV preparation," incubated for 15 min on ice, and subsequently centrifuged at 15,000×*g* for 15 min at 4 °C. For the cell protein analysis, the cells were washed with ice-cold PBS (pH 7.4), incubated in 60 μL lysis buffer (as described above), scraped, transferred to a centrifugation tube, and centrifuged at 15,000×*g* for 15 min at 4 °C. Subsequently, the supernatant collected from the EV preparation and ChPE cells was transferred to a low protein–binding microtube (72.706.600, Sarstedt, Nümbrecht, Germany) and stored at −80 °C. The presence of IGF-1 in EVs derived from human CSF, in mice ChPE cells supernatant, and in ChPE cells was determined using the Human IGF-1 ELISA (Mediagnost, Reutlingen, Germany) according to the manufacturer's instructions.

Immunofluorescence microscopy and image analysis

Primary ChPE cells were fixed in 4% buffered paraformaldehyde (PFA prepared in PBS, pH 7.4) for 15 min and washed three times with PBS. The cells were thereafter permeabilized with 0.1% TritonX-100 (diluted in PBS, Invitrogen, Waltham, MA, USA) for 10 min, subsequently blocked with 10% FBS for 1 h, and incubated with primary and secondary antibodies (as described below) overnight at 4 °C and for 1 h at room temperature, respectively. The following primary antibodies were used: Hsp47 (1:200, rabbit antimouse, ab109117, Abcam, Cambridge, United Kingdom), S100A4 (1:250, rabbit antimouse; ab197896, Abcam), IGF-1 (1:100, Rabbit antimouse, bs-0014R, Bioss, Woburn, MA, USA), IGF-1 (1:100, goat antimouse, AF791, R&D systems), IGF-1R (1:20, goat antimouse, AF-305-NA, R&D systems), ZO-1 (1:50, rabbit antimouse, 61-7300, Thermo Fisher Scientific, Waltham, MA, USA), donkey antigoat 647 (1:500, A-21447, Thermo Fisher Scientific), TTR (1:50, sheep antimouse, ab9015, Abcam), and CD63 (1:100, rabbit antimouse, ab217345, Abcam). The following secondary antibodies were used with the corresponding primary antibody: donkey antigoat 488 (1:500, A-11015, Thermo Fisher Scientific), goat antirabbit 488 (1:500, ab150077, Abcam), goat antirabbit 568 (1:500, ab175471, Abcam), and donkey antisheep 488 (1:400, A-11015, Thermo Fisher Scientific). The membranes were counterstained with Hoechst (1:10,000 in DMSO, H1398, Invitrogen) for 5 min at room temperature and mounted using mounting media (Merck). To visualize the samples, a Nikon Confocal A1RHD confocal (Nikon) microscope was used.

Electron microscopy

ChPE cell–derived EVs were prepared as described in "EV preparation." Subsequently, 30 μL of an EV preparation was fixed with 30 μL 4% PFA for 30 min at room temperature. A drop (~5 μL) of fixed EV suspension was placed on a Formvar–carbon-coated electron microscopy grid (Ted Pell, Redding, CA, USA) to air-dry for 20 min at room temperature. Next, to wash the samples, the grid was placed to float over a drop of 100 μL PBS placed on clean parafilm surface. All subsequent steps were performed in the same manner. The grids were blocked with 1% bovine serum albumin (BSA, diluted in PBS) and incubated with primary antibody against IGF-1 (1:100, rabbit antimouse, bs-0014R, Bioss) and flotillin 2 (5 μg/mL, rabbit antimouse, ab96507, Abcam) for 120 min at room temperature. Incubation with secondary antibody, goat antirabbit IgG (H+L) 10 nm gold conjugate (1:20, 17010-1, Ted Pella), was performed for 60 min at room temperature.

ChPE cells cultured as described in "Primary ChPE cell cultures" were prefixed with 4% PFA for 1 h and subsequently rinsed several times with Sorensen phosphate buffer (0.1 M). Cells were thereafter dehydrated with acetone in distilled water in a six-step series with increased acetone concentration per step (30–100%). Time per step was 5–10 min. Cells were then impregnated overnight with a 1:1 mixture of acetone and Epon (Agar Scientific Ltd, Stansted, Essex, United Kingdom). Next, the cells were embedded in Epon, then polymerized for 48 h at 60 °C, and ultrathin sectioned (60 nm thick). Blocking was subsequently conducted for 1 h using 1% BSA in distilled water, and cells were incubated with primary antibodies against IGF-1 (1:100, goat antimouse, AF791, R&D systems, or 1:100, goat antihuman, AF291, R&D systems) and flotillin 2 (10 μg/mL, rabbit antimouse, ab96507, Abcam) overnight at 4 °C. Incubation with secondary antibodies, rabbit antigoat IgG (H+L) 10 nm gold conjugate (1:20, 17410-1, Ted Pella) and goat antirabbit IgG (H+L) 10 nm gold conjugate (1:20, 17010-1, Ted Pella), was performed for 60 min at room temperature. The sections were stained with uranyl acetate (4%, Agar scientific) for 20 min at 38 °C. All samples, both EVs and ChPE cells, were examined in a FEI Technai Biotwin 120 kv (FEI, Hillsboro, OR,

USA) TEM operated at 100 kV accelerating voltage (FEI). Images were recorded with a side-mounted Olympus Veleta camera with a resolution of 2,048 × 2,048 pixels (FEI).

Liquid chromatography–MS

Samples were prepared for MS analysis as described previously (10). 100 µL Ripa buffer (R0278, Sigma-Aldrich) was added to samples prepared as described in "EV preparation," followed by sonication for 40 cycles (15 s on, 15 s off) using a Bioruptor (Diagenode, Denville, NJ, USA). Samples were reduced with DTT to a final concentration of 10 mM and heated at 56 °C for 30 min, followed by alkylation with iodoacetamide to a final concentration of 20 mM for 30 min at room temperature in the dark. Samples were precipitated overnight with ice-cold ethanol (final ethanol concentration 90%) at −20 °C followed by centrifugation at 14,000×*g* for 10 min. The resulting pellets were air-dried, resuspended in 50 µL of 100 mM ammonium bicarbonate, and sonicated using a Bioruptor (Diagenode), 40 cycles (15 s on, 15 s off). Protein concentration was measured at 280 nm using a NanoDrop (DeNovix DS-11, DeNovix Inc; Wilmington, DE, USA). Digestion was performed by adding trypsin in a ratio of 1:50 (sequencing grade modified trypsin, part no. V511A, Promega, Madison, WI, USA) to the samples and incubating overnight at 37 °C. The digestion was stopped with 5 µL 10% trifluoroacetic acid. The samples were Speed Vac to dryness and redissolved in 2% ACN (0.1%).

Solubilized peptides were analyzed on an Exploris 480 mass spectrometer (Thermo Fischer Scientific) coupled with a Vanquish Neo UHPLC system (Thermo Fischer Scientific). A two-column setup was used on the HPLC system, and peptides were loaded into an Acclaim PepMap 100 C18 precolumn (75 µm × 2 cm, Thermo Scientific) and then separated on an EASY spray column (75 µm × 25 cm, C18, 2 µm, 100 Å, ES902) with a flow rate of 300 nL/min. The column temperature was set at 45 °C. Solvent A (0.1% FA in water) and solvent B (0.1% FA in 80% ACN) were used to create a 90-min nonlinear gradient from 5 to 25% of solvent B for 75 min, which was then increased to 32% for 9 min and finally to 45% for 6 min to elute the peptides.

The samples were analyzed with data-dependent acquisition (DDA) in positive mode. The full MS spectra 1 (MS1) resolution was set to 120,000 at m/z 200, and the normalized AGC target was set to 300% with a maximum injection time of 45 ms. The full mass range was set to 375–1500 m/z. Precursors were isolated with the isolation window of 1.3 m/z and fragmented by HCD with the normalized collision energy of 30. The full MS spectra 2 (MS2) was detected in the Orbitrap with a resolution of 15,000. The normalized AGC target and the maximum injection time were set to 100% and custom, respectively. The intensity threshold for precursor selection was set to 1e4, and 40-s dynamic exclusion was applied.

Analysis of MS data

The raw DDA data were analyzed as described previously (10), with Proteome Discoverer 2.5 Software (Thermo Fisher Scientific), and with peptide identification carried out using SEQUEST HT against the UniProtKB Mouse and Pig canonical databases (UP000000589 and UP000008227, respectively), as well as fasta files for human IGF-1 (P05019). The search was performed with the following parameters applied: carbamidomethylation of cysteine as a static modification and N-terminal acetylation and methionine oxidation as dynamic modifications. Precursor mass tolerance was set at 10 ppm and fragment mass tolerance at 0.02 Da. Up to two missed cleavages were permitted, and peptide validation was conducted using Percolator with a maximum *q*-value of 0.01. Identified peptides were quantified by label-free relative quantification, and extracted chromatographic intensities were used to compare peptide abundance across samples.

Protein abundancies were submitted to the online tool Proteomill (https://github.com/martinry/ProteoMill) (47). Missing values were set so that each protein had a minimum of six values in each group. Enrichment analysis was performed by searching the GO, David, and Metascape databases for Reactome pathways and GO terms (26–28, 48).

In vivo intraventricular brain injections

EVs prepared as described in "IGF-1 exposure of CPE cell cultures" and "EV preparation" were stained with PKH26 Red Fluorescent Cell Linker Mini Kit for General Cell Membrane Labeling (Merck, MINI26) as described by the manufacturer. Briefly, 400 µL of ChPE supernatant was mixed with PBS and PKH26 (1:200) in a total volume of 800 µL and subsequently incubated for 20 min at room temperature. This was followed by exosome isolation as described in "EV preparation" and pellet resuspension in 50 µL PBS. Guided by high-frequency ultrasound (Vevo 2100, VisualSonics Inc., ON, Canada) using a MS-550D 40 MHz transducer, nonsedated preterm rabbit pups at a postnatal age of 24 h received an i.c.v. injection of 25 µL stained EVs using a BD Microfine+0.3 mL (30 gauge). After 4.5 h, the pups were anesthetized with an intramuscular injection of Ketaminol Vet. (50 mg/mL, Intervet AB, Stockholm, Sweden) and Rompun Vet. (20 mg/mL, Bayer Animal Health, Leverkusen, Germany) in combination with isoflurane inhalation (Attane Vet., 1,000 mg/g, VM Pharma AB, Stockholm, Sweden) and subsequently transcardially perfused with freshly prepared PBS (containing heparin 1000 IU/mL), followed by perfusion with freshly prepared 4% PFA (VWR Chemicals, Leuven, Belgium) buffered with PBS (pH 7.4). After fixation, the brains were extracted from the skull and post-fixed by immersion in 4% PFA. A change to fresh PFA was performed after 6–8 h, and brains were then immersed in PFA for a total of 24 h at 4 °C and transferred to PBS for further processing as described below.

Histological detection of administrated EVs in the brain of preterm rabbit pups

Brains were divided in two pieces through a coronal section in the midbrain (close to the location of the subfornical organ) and then incubated in 4% PFA for 4 h at room temperature. Next, brains were rinsed with PBS (pH 7.4) for 8 h at 4 °C, embedded in OCT cryomount (Histolab, Göteborg, Sweden) and frozen on dry ice in isopentane. Cryosections (10 µm thick) collected at the level of the midbrain, containing the lateral and central ventricles with the ChP and the hippocampus, were collected on SuperFrost Plus slides (Gerhard Menzel B.V. & Co., Braunschweig, Germany). Following rinses with PBS (2 × 5 minutes), sections (3–6 per animal) were incubated with 4′,6-diamidino-2-phenylindole (DAPI) for 15 min at room temperature and subsequently mounted and cover-slipped in Fluoroshield antifade mounting media (Abcam). Analysis was performed with a confocal laser scanning microscope (Zeiss LSM 800, ZEIZZ, Oberkochen, Germany). Detection of PKH26 (stained vesicles) was performed with excitation maxima at 551 nm and emission maxima at 567 nm. Sequential scanning was performed of PKH26 and DAPI for analysis of the distribution and location of PKH26 fluorescence, primarily in the ChP, ventricular brain ependyma, and the parenchyma of the hippocampus. Both hemispheres were analyzed. Threshold detection level of PKH26 was set in brain sections from animals that received only the dye (no vesicles). Representative images were taken and converted to TIFF format for illustrations.

In vitro hippocampal neuron EV uptake

Wistar rats were obtained from Charles River (Sulzfeld, Germany) and handled in accordance with the Danish Animal Welfare Act approved by the Department of Experimental Medicine at the University of Copenhagen (Project no. P20-070). Primary hippocampal neurons were isolated from embryonic day 19 Wistar rat embryos in accordance with previous description (49). Dissected hippocampi were chopped in ice-cold Krebs–Ringer buffer (KRB, Invitrogen) and treated with 0.1% (w/v) trypsin for 6–7 min at 37 °C, followed by incubation with 0.052% (v/w) trypsin inhibitor and 0.008% (v/w) DNase I diluted in KRB. Undissociated tissue was pelleted by centrifugation, and the neurons were resuspended in KRB containing 0.13 mM Ca^{2+} and 2.4 mM Mg^{2+} (Invitrogen). Cells were pelleted by centrifugation and resuspended in Neurobasal medium supplemented with 2% (v/v) B27, 100 U/mL penicillin, and 100 μg/mL streptomycin (all from Invitrogen). Neurons were then plated at a density of 5×10^4 cells/cm^2 in 8-well LabTek Permanox chamber slides (Nunc, Roskilde, Denmark) precoated with 20 μg/mL poly-L-lysine and cultured for 8–10 days with 50% medium exchange at the second and seventh days of culture. For the uptake experiment, ChPE cell–derived EVs were stained with PKH67 Green Fluorescent Cell Linker Mini Kit for General Cell Membrane Labeling as described by the manufacturer (Merck, MINI67). Briefly, 400 μL of ChPE supernatant was mixed with PBS and PKH67 (1:200) in a total volume of 800 μL and subsequently left to incubate for 20 min at room temperature. This was followed by exosome isolation as described in "EV preparation" and pellet resuspension in 300 μL PBS. Subsequently, neurons were stimulated for 2 h with the PKH67-stained EVs. For each slide, a well with unstimulated cells was used as control, and wells with only PKH67-stained supernatant with no cells were used as negative control. Cells were then washed with PBS, fixed with 4% PFA for 20 min, blocked with 5% BSA, and labeled with polyclonal rabbit antirat growth-associated protein-43 (GAP-43) antibody (1:1,000; Millipore) overnight at 4 °C followed by incubation with secondary goat antimouse AF 546-conjugated antibodies (1:1000; Invitrogen). For visualization of nuclear morphology, cells were counterstained with Hoechst 33258 (1:1000; Invitrogen) and slides were mounted with antifade mounting medium (Dako, Glostrup, Denmark). Analyses and representative images were grabbed in systematic series of fields of view across the whole area of a well using a ZEIZZ confocal laser scanning microscope (ZEIZZ LSM800, ZEIZZ).

For PKH67 fluorescence analysis, slides were evaluated manually. Focus was set manually for each image required. To obtain digital images, a wide-field epi-fluorescence microscope (Olympus IX70, Tokyo, Japan) equipped with a digital detector (DP80, Olympus) was used under fixed lighting conditions and regions of interest were manually annotated. Images were imported to ImageJ version 2.9.0 for quantitative analysis. Quantification of green signal (PKH67) per number of nuclei was used to determine fluorescence. A script was developed for ImageJ in order to conduct the analysis of the captured fluorescence images. The images contained two channels: DAPI (blue) and PKH67 (green). The DAPI channel threshold was set manually to count the number of cell nuclei, and the green channel was used to capture the area of PKH67 labeling. The result was diagrammed as the quotient of the PKH67 labeled area in relation to the number of cell nuclei.

Sex determination

Determinations of rabbit sex were performed by confirming the presence of the sex-determining region of the Y gene (gene ID: 100,328,958) in the rabbit genome using PCR and gel electrophoresis visualization as described before (10, 50). Briefly, DNA was extracted from an ear biopsy using DNeasy Blood and Tissue Kit (Qiagen) according to the manufacturer's instructions. One μL of DNA (range: 100–200 ng/μL) was used in the PCR (30 cycles at 57 °C) with the following primers: sense: TGCAATACAGGAGGAACACG, antisense: AGCAAACTGTCGCTCTTCTG. Presence of a band at ∼299 bp determined the animal as male, and no corresponding band determined the animal as female.

Statistics

Statistical significance was calculated using one-way ANOVA with a post hoc Tukey test for multiple comparisons of means, or Student's t test for pairwise comparisons. P-value < 0.05 was considered significant. Data are presented as means ± SD. Statistical analyses were performed using R version 4.3.1.

Acknowledgments

The authors acknowledge Lina Gefors and Sebastian Wasserström, Lund University Bioimaging Center, for providing technical assistance and scientific support related to the TEM and confocal microscopy. In addition, the authors acknowledge Charlotte Welinder, Center of Excellence in Biological and Medical Mass Spectrometry at Lund University, for conducting the MS experiments. The authors also acknowledge Anders Brinte for providing assistance in the fluorescence analysis and Pia Ecke, Imagene-iT AB, for histological work related to the confocal microscopy analyses.

Supplementary Material

Supplementary material is available at *PNAS Nexus* online.

Funding

The research was funded by the Swedish Research Council (Grant No. 2020-01235), Governmental ALF research grants to Lund University and Skåne University Hospital, the Crafoord Foundation, the Alfred Österlund Foundation, and Takeda Pharmaceutical Company Ltd.

Author Contributions

N.O., D.L., and M.G. designed the study. N.O., S.V., H.K., C.E., A.K., B.H., S.P., and M.G. conducted the study and acquired the data. N.O., B.H., S.P., N.B., D.L., and M.G. analyzed and interpreted the data. N.O. and M.G. wrote the manuscript. All authors read, critically reviewed, and approved the manuscript and are consequently in agreement to be accountable for all aspects of this work.

Data Availability

All data are presented within the manuscript or are available in the Supplementary Materials, including the raw MS data.

References

1 Gubbi S, Quipildor GF, Barzilai N, Huffman DM, Milman S. 2018. 40 YEARS of IGF1: IGF1: the Jekyll and Hyde of the aging brain. *J Mol Endocrinol*. 61:T171–T185.

2 Hellström A, *et al.* 2016. Role of insulinlike growth factor 1 in fetal development and in the early postnatal life of premature infants. *Am J Perinatol*. 33:1067–1071.

3 Hansen-Pupp I, *et al.* 2011. Postnatal decrease in circulating insulin-like growth factor-I and low brain volumes in very preterm infants. *J Clin Endocrinol Metab*. 96:1129–1135.
4 Hansen-Pupp I, *et al.* 2013. Circulatory insulin-like growth factor-I and brain volumes in relation to neurodevelopmental outcome in very preterm infants. *Pediatr Res*. 74:564–569.
5 Fernandez AM, Torres-Alemán I. 2012. The many faces of insulin-like peptide signalling in the brain. *Nat Rev Neurosci*. 13:225–239.
6 Christiansen LI, *et al.* 2023. Insulin-like growth factor-1 supplementation promotes brain maturation in preterm pigs. *eNeuro*. 10:ENEURO.0430-22.2023.
7 Ley D, *et al.* 2019. rhIGF-1/rhIGFBP-3 in preterm infants: a phase 2 randomized controlled trial. *J Pediatr*. 206:56–65.e58.
8 Carro E, Nuñez A, Busiguina S, Torres-Aleman I. 2000. Circulating insulin-like growth factor I mediates effects of exercise on the brain. *J Neurosci*. 20:2926–2933.
9 Bolós M, Fernandez S, Torres-Aleman I. 2010. Oral administration of a GSK3 inhibitor increases brain insulin-like growth factor I levels. *J Biol Chem*. 285:17693–17700.
10 Ortenlöf N, *et al.* 2023. Characterization of choroid plexus in the preterm rabbit pup following subcutaneous administration of recombinant human IGF-1/IGFBP-3. *Fluids Barriers CNS*. 20:59.
11 Lun MP, Monuki ES, Lehtinen MK. 2015. Development and functions of the choroid plexus-cerebrospinal fluid system. *Nat Rev Neurosci*. 16:445–457.
12 Gram M, *et al.* 2021. Insulin-like growth factor 1 in the preterm rabbit pup: characterization of cerebrovascular maturation following administration of recombinant human insulin-like growth factor 1/insulin-like growth factor 1-binding protein 3. *Dev Neurosci*. 43:281–295.
13 Grapp M, *et al.* 2013. Choroid plexus transcytosis and exosome shuttling deliver folate into brain parenchyma. *Nat Commun*. 4:2123.
14 Balusu S, *et al.* 2016. Identification of a novel mechanism of blood-brain communication during peripheral inflammation via choroid plexus-derived extracellular vesicles. *EMBO Mol Med*. 8:1162–1183.
15 Cruz L, Romero JAA, Iglesia RP, Lopes MH. 2018. Extracellular vesicles: decoding a new language for cellular communication in early embryonic development. *Front Cell Dev Biol*. 6:94.
16 Kalra H, Drummen GP, Mathivanan S. 2016. Focus on extracellular vesicles: introducing the next small big thing. *Int J Mol Sci*. 17:170.
17 Menheniott TR, Charalambous M, Ward A. 2010. Derivation of primary choroid plexus epithelial cells from the mouse. *Methods Mol Biol*. 633:207–220.
18 Kratzer I, Ek J, Stolp H. 2020. The molecular anatomy and functions of the choroid plexus in healthy and diseased brain. *Biochim Biophys Acta Biomembr*. 1862:183430.
19 Strutz F, *et al.* 1995. Identification and characterization of a fibroblast marker: FSP1. *J Cell Biol*. 130:393–405.
20 Miyamura T, *et al.* 2020. Small molecule inhibitor of HSP47 prevents pro-fibrotic mechanisms of fibroblasts in vitro. *Biochem Biophys Res Commun*. 530:561–565.
21 Srinivasan B, *et al.* 2015. TEER measurement techniques for in vitro barrier model systems. *J Lab Autom*. 20:107–126.
22 Andreu Z, Yáñez-Mó M. 2014. Tetraspanins in extracellular vesicle formation and function. *Front Immunol*. 5:442.
23 Trajkovic K, *et al.* 2008. Ceramide triggers budding of exosome vesicles into multivesicular endosomes. *Science*. 319:1244–1247.
24 Aber R, Chan W, Mugisha S, Jerome-Majewska LA. 2019. Transmembrane emp24 domain proteins in development and disease. *Genet Res (Camb)*. 101:e14.
25 Holgersen K, *et al.* 2022. Clinical outcome and gut development after insulin-like growth factor-1 supplementation to preterm pigs. *Front Pediatr*. 10:868911.
26 Zhou Y, *et al.* 2019. Metascape provides a biologist-oriented resource for the analysis of systems-level datasets. *Nat Commun*. 10:1523.
27 Gillespie M, *et al.* 2021. The reactome pathway knowledgebase 2022. *Nucleic Acids Res*. 50:D687–D692.
28 Ashburner M, *et al.* 2000. Gene ontology: tool for the unification of biology. The Gene Ontology Consortium. *Nat Genet*. 25:25–29.
29 Kalra H, *et al.* 2012. Vesiclepedia: a compendium for extracellular vesicles with continuous community annotation. *PLoS Biol*. 10: e1001450.
30 Pathan M, *et al.* 2019. Vesiclepedia 2019: a compendium of RNA, proteins, lipids and metabolites in extracellular vesicles. *Nucleic Acids Res*. 47:D516–D519.
31 Bach LA, Headey SJ, Norton RS. 2005. IGF-binding proteins–the pieces are falling into place. *Trends Endocrinol Metab*. 16:228–234.
32 Hellstrom A, *et al.* 2017. IGF-1 as a drug for preterm infants: a step-wise clinical development. *Curr Pharm Des*. 23:5964–5970.
33 Schwerk C, Tenenbaum T, Kim KS, Schroten H. 2015. The choroid plexus—a multi-role player during infectious diseases of the CNS. *Front Cell Neurosci*. 9:80.
34 Pulford BE, Ishii DN. 2001. Uptake of circulating insulin-like growth factors (IGFs) into cerebrospinal fluid appears to be independent of the IGF receptors as well as IGF-binding proteins. *Endocrinology*. 142:213–220.
35 Pan WH, Kastin AJ. 2000. Interactions of IGF-1 with the blood-brain barrier in vivo and in situ. *Neuroendocrinology*. 72:171–178.
36 Carro E, Spuch C, Trejo JL, Antequera D, Torres-Aleman I. 2005. Choroid plexus megalin is involved in neuroprotection by serum insulin-like growth factor I. *J Neurosci*. 25:10884–10893.
37 Thompson AG, *et al.* 2018. UFLC-Derived CSF extracellular vesicle origin and proteome. *Proteomics*. 18:e1800257.
38 Vandendriessche C, *et al.* 2021. Importance of extracellular vesicle secretion at the blood–cerebrospinal fluid interface in the pathogenesis of Alzheimer's disease. *Acta Neuropathol Commun*. 9:143.
39 Fricke F, Gebert J, Kopitz J, Plaschke K. 2021. Proinflammatory extracellular vesicle-mediated signaling contributes to the induction of neuroinflammation in animal models of endotoxemia and peripheral surgical stress. *Cell Mol Neurobiol*. 41:1325–1336.
40 Slupe AM, Kirsch JR. 2018. Effects of anesthesia on cerebral blood flow, metabolism, and neuroprotection. *J Cereb Blood Flow Metab*. 38:2192–2208.
41 Wei Z, *et al.* 2023. Toward accurate cerebral blood flow estimation in mice after accounting for anesthesia. *Front Physiol*. 14:1169622.
42 Romantsik O, *et al.* 2022. Severe intraventricular hemorrhage causes long-lasting structural damage in a preterm rabbit pup model. *Pediatr Res*. 92:403–414.
43 van der Merwe J, *et al.* 2021. Earlier preterm birth is associated with a worse neurocognitive outcome in a rabbit model. *PLoS One*. 16:e0246008.
44 Romantsik O, *et al.* 2019. The heme and radical scavenger α(1)-microglobulin (A1 M) confers early protection of the immature brain following preterm intraventricular hemorrhage. *J Neuroinflammation*. 16:122.
45 Sveinsdóttir K, *et al.* 2017. Impaired cerebellar maturation, growth restriction, and circulating insulin-like growth factor 1 in preterm rabbit pups. *Dev Neurosci*. 39:487–497.
46 Sveinsdóttir S, Cinthio M, Ley D. 2012. High-frequency ultrasound in the evaluation of cerebral intraventricular haemorrhage in preterm rabbit pups. *Ultrasound Med Biol*. 38:423–431.

47 Rydén M, Englund M, Ali N. 2021. ProteoMill: efficient network-based functional analysis portal for proteomics data. *Bioinformatics*. 37: 3491–3493.

48 Sherman BT, *et al.* 2022. DAVID: a web server for functional enrichment analysis and functional annotation of gene lists (2021 update). *Nucleic Acids Res*. 50:W216–W221.

49 Pankratova S, *et al.* 2016. Immunomodulator CD200 promotes neurotrophic activity by interacting with and activating the fibroblast growth factor receptor. *Mol Neurobiol*. 53:584–594.

50 Hellström A, *et al.* 2016. Insulin-like growth factor 1 has multisystem effects on foetal and preterm infant development. *Acta Paediatr*. 105: 576–586.